HHS Public Access

Author manuscript

Proteomics. Author manuscript; available in PMC 2016 January 01.

Published in final edited form as:

Proteomics. 2015 January ; 15(0): 327–339. doi:10.1002/pmic.201400200.

Phosphoproteomic analysis of basal and therapy-induced adaptive signaling networks in *BRAF* and *NRAS* mutant melanoma

Inna V. Fedorenko[1], **Bin Fang**[2], **A. Cecelia Munko**[1], **Geoffrey T. Gibney**[3], **John M. Koomen**[1], and **Keiran S.M. Smalley**[1,3,*]

[1]The Department of Molecular Oncology, The Moffitt Cancer Center & Research Institute, 12902 Magnolia Drive, Tampa, FL, 33612

[2] Proteomics, The Moffitt Cancer Center & Research Institute, 12902 Magnolia Drive, Tampa, FL, 33612

[3]The Department of Cutaneous Oncology, The Moffitt Cancer Center & Research Institute, 12902 Magnolia Drive, Tampa, FL, 33612

Abstract

Basal and kinase inhibitor-driven adaptive signaling has been examined in a panel of melanoma cell lines using phosphoproteomics in conjunction with pathway analysis. A considerable divergence in the spectrum of tyrosine-phosphorylated peptides was noted at the cell line level. The unification of genotype-specific cell line data revealed the enrichment for the tyrosine-phosphorylated cytoskeletal proteins to be associated with the presence of a *BRAF* mutation and oncogenic *NRAS* to be associated with increased receptor tyrosine kinase phosphorylation. A number of proteins including cell cycle regulators (CDK1, CDK2 and CDK3), MAPK pathway components (ERK1 and ERK2), interferon regulators (TYK2), GTPase regulators (RIN1) and controllers of protein tyrosine phosphorylation (DYR1A and PTPRA) were common to all genotypes. Treatment of a *BRAF*-mutant/PTEN-null melanoma cell line with vemurafenib led to decreased phosphorylation of ERK, phospholipase C1 and β-catenin with increases in RTK phosphorylation, STAT3 and GSK3α noted. In *NRAS*-mutant melanoma, MEK inhibition led to increased phosphorylation of EGFR signaling pathway components, Src family kinases and PKCδ with decreased phosphorylation seen in STAT3 and ERK1/2. Together these data present the first systems level view of adaptive and basal phosphotyrosine signaling in *BRAF*- and *NRAS*-mutant melanoma.

Keywords

melanoma; BRAF; NRAS; signaling; phosphoproteomics

*To whom correspondence should be addressed Tel: 813-745-8725, Fax: 813-449-8260, keiran.smalley@moffitt.org.

Introduction

Melanoma continues to lead the field of targeted cancer therapy, with remarkable responses being seen in *BRAF*-mutant melanoma patients following treatment with BRAF and/or MEK inhibitors [1, 2]. Despite this, responses to these regimens are relatively short-lived (progression-free survival 5.8 months and 9.6 months for BRAF inhibitor monotherapy and BRAF/MEK inhibitor therapy, respectively) with resistance being nearly inevitable [1, 3]. The success of BRAF inhibitors in melanoma has led to therapies being selected on the basis of the driver oncogene [4]; 50% of all cutaneous melanomas are known to harbor activating *BRAF* mutations, with the majority of these being a valine to glutamic acid substitution (the V600E mutation) [5]. Other categories include 15-20% of melanomas driven through oncogenic *NRAS* (mostly mutation at the Q61 position) and ~30% of tumors having no obvious driver mutation (*BRAF/NRAS* wild-type melanomas) [6, 7]. For melanoma patients whose tumors lack *BRAF* mutations, targeted therapy options are very limited. Although there is some evidence that MEK inhibitors have some activity in *NRAS*-mutant melanoma, response rates and the durability of responses are low [7, 8]. No targeted therapeutic options have yet been identified for melanoma patients whose tumors are *BRAF/NRAS* wild-type [9].

Melanomas have one of the highest mutational loads of all cancers, with the majority of these arising from UV-radiation exposure [6]. Attempts to understand melanoma biology on a systems level have mostly focused upon large-scale whole exome sequencing studies [6, 10]. Although these studies have identified important new melanoma oncogenes and have shed light upon mechanisms of acquired BRAF and BRAF/MEK inhibitor resistance, little insight has been gained into the differences in intracellular signaling between the four molecular classifications of melanoma mutation status: *BRAF*, *NRAS*, *BRAF/NRAS* and wild-type [3, 11].

Adaptation to kinase inhibitor therapy is a critical step that allows minor populations of cells to escape from therapy and remain dormant until secondary resistance-mediating mutations can be acquired [12, 13]. Work from our lab and others has shown that treatment of *BRAF*-mutant melanoma cells with the BRAF inhibitors PLX4720 and vemurafenib leads to recovery of MAPK signaling that allows for therapeutic escape [13, 14]. Dual targeting with a combination of either a BRAF and a MEK inhibitor or a BRAF and a HSP90 inhibitor prevents the adaptive recovery of signaling, leading to more durable therapeutic responses [1, 14-16]. Although phosphoproteomics has been previously used to characterize the DNA damage response and the response of melanoma cells to MEK inhibition, only limited numbers of cell lines were profiled [17, 18]. The goal of the present study was to gain a more in-depth understanding of both the basal, oncogene-specific signaling networks and the mechanisms of therapeutic adaptation that will permit the identification of new therapeutic vulnerabilities. For that purpose, we have utilized phosphotyrosine immunoprecipitation, LC-MS/MS, label-free quantification, and pathway mapping to explore the basal and adaptive signaling in melanoma cell lines to explore the responses to current targeted therapeutics (e.g. BRAF and MEK inhibitors) [19, 20].

Materials and Methods

Cell culture and reagents

The 1205Lu, WM9, WM793, WM164, WM983A, WM239, WM209, WM39, WM1346, WM1366, WM1361A, WM2032, WM3970, and WM3929 melanoma cells lines were a generous gift from Dr. Meenhard Herlyn (The Wistar Institute, Philadelphia, PA). The identity and purity of each cell line was confirmed by Biosynthesis Inc. (Lewisville, TX) through STR validation analysis. Cell lines were maintained in RPMI-1640 (Mediatech, Manassas, VA) supplemented with 5% FBS (Sigma Aldrich, St. Louis, MO).

Phosphoproteomic sample preparation and LC-MS/MS

For each cell line, 1×10^8 cells (~10mg total protein) were used. The cells were treated for 24 hours prior to collection with 3 mM Vemurafenib (Plexxikon, Berkeley, CA) for BRAF inhibition and 10 mM U0126 (EMD Millipore, Billerica, MA) for MEK inhibition. Cells were lysed in denaturing buffer containing 8 M Urea, 20 mM HEPES pH 8, 1 mM sodium orthovanadate, 2.5 mM sodium pyrophosphate and 1 mM β-glycerophosphate. The proteins were reduced with 4.5 mM DTT for 20 minutes at 60º C and alkylated with 10 mM iodoacetamide for 15 minutes. Trypsin (Worthington, Lakewood, NJ) digestion was carried out at room temperature overnight with enzyme to substrate ratio of 1:100. Tryptic peptides were then acidified with 1% trifluoroacetic acid (TFA) and desalted with C18 Sep-Pak cartridges according to the manufacturer's suggested protocol (Waters, Milford, MA). Following lyophilization, the dried peptide pellet was re-dissolved in IAP buffer containing 50 mM MOPS pH 7.2, 10 mM sodium phosphate and 50 mM sodium chloride. Phosphotyrosine-containing peptides were immunoprecipitated with immobilized anti-phosphotyrosine antibody, p-Tyr-100. (Cell Signaling Technology) [19]. After overnight incubation, the antibody beads were washed 3 times with IAP buffer, followed by 2 washes with deionized H_2O. The phosphotyrosine peptides were eluted twice with 0.15% TFA, and the volume was reduced to 20 µl via vacuum centrifugation. In peptide sequencing experiments, a nanoflow liquid chromatograph (U3000, Dionex, Sunnyvale, CA) coupled to an electrospray ion trap mass spectrometer (LTQ-Orbitrap, Thermo, San Jose, CA) was used for tandem mass spectrometry peptide sequencing experiments. The sample was first loaded onto a pre-column (5mm × 300 µm ID packed with C18 reversed-phase resin, 5µm, 100Å) and washed for 8 minutes with aqueous 2% acetonitrile with 0.04% trifluoroacetic acid. The trapped peptides were then eluted onto the analytical column, (75 µm ID × 15 cm length, C18 PepMap 100, Dionex, Sunnyvale, CA). The 120-minute gradient was programmed using solvent A (2% acetonitrile + 0.1% formic acid) and solvent B (90% acetonitrile + 0.1% formic acid) delivered at 300 nl/min. After loading and washing at 5% B for 8 minutes, the gradient was applied from 5% to 50% B over 90 minutes, increasing from 50% to 90% B in 7 minutes, and held at 90% for 5 minutes to wash the column. Re-equilibration was achieved by decreasing solvent B from 90% to 5% in 1 minute for re-equilibration at 5% B for 10 minutes. Five tandem mass spectra were collected in a data-dependent manner following each survey scan. MS scans were acquired in the orbital ion trap to obtain accurate peptide mass measurements, and the MS/MS scans were acquired in the linear ion trap using 60 second exclusion for previously sampled peptide peaks. Each sample was analyzed in duplicate.. Sequest (Thermo, San Jose, CA) and Mascot

(www.matrixscience.com) searches were performed against human entries in the UniProt database. The precursor mass tolerance was set at 1.08 Da, and fragment ion mass tolerance was set at 0.8 Da. Dynamic modifications included carbamidomethylation (Cys, +57.021464), oxidation (Met, +15.994915) and phosphorylation (Ser/Thr/Tyr, +79.966331), and as many as 2 missed tryptic cleavages were allowed. Both MASCOT and SEQUEST search results were summarized in Scaffold 3.0 (www.proteomesoftware.com). MaxQuant (v. 1.2.2.5) was used for label-free quantification with peptide and modification site FDR values set to 0.05 [21, 22]. For manual verification, integrated peak areas for pY peptide quantification were analyzed from extracted ion chromatograms (EIC) using QuanBrowser from Xcalibur 2.0 with m/z tolerance +/− 0.02 and retention time tolerance +/− 2 minutes. Raw data and Scaffold files are available through PeptideAtlas (Identifier: PASS00559).

Western blotting

Western blotting was performed as previously described in [23]. Antibodies for phospho-ERK, total ERK, phospho-MEK, total MEK, phospho-AKT and total AKT were from Cell Signaling Technology (Danvers, MA). Antibody to β-actin was purchased from Sigma Aldrich (St. Louis, MO).

Immunofluorescence

WM1346 cells were grown on glass coverslips overnight then treated with either vehicle or U0126 (10 μM, 24 hrs.). Cells were then fixed using 4% paraformaldehyde, permeabilized with 0.2% Triton-X100 and incubated with Texas-Red phalloidin (Invitrogen, Carlsbad, CA) for 1 hr. at 37C. Cells were imaged as described in [23].

Flow cytometry

Cells were plated at 60% confluency and allowed to attach overnight in 6-well plates. Cultures were then treated with vehicle, 3μM vemurafenib, 3μM GDC-0941 (Selleck) or the combination of 3μM vemurafenib and 3μM GDC-0941 for 72 hours. Annexin V and TMRM staining was performed as previously described in [24].

Growth inhibition assays

MTT assays with U0126 or vemurafenib were performed as described in [23]. Cells were treated for 72 hours. Data show the mean of three independent experiments ± the S.E. of the mean.

Kinome arrays

Relative phosphorylation levels of forty-three phosphorylation sites on human kinases were quantified using the Proteome Profiler Human Phospho-Kinase Array Kit (R&D Systems) following the manufacturer's protocol (ARY003).

Wound Scratch Assay

Cells were plated in 6-well plates and grown to confluency. A uniform scratch was made in the confluent cell layer using a P200 pipette tip. Cells were treated with either vehicle or U0126 (10 μM, 24 hrs.) before being allowed to grow for 24 hrs.

Data Processing

In order to identify the proteins that have the highest tyrosine phosphorylation intensities across the basal panel of cell lines in instances where multiple quantified peptides mapped to a single protein, the pY intensities of these peptides were averaged per protein. To focus on the specific phosphorylation changes during adaptive signaling, when multiple quantified peptides mapped to a single protein, the peptides with the highest pY intensities were used for pathway mapping and network analysis (same peptide compared among basal and treated sample quantifications).

Heat Maps and Metacore Analysis

Heat maps of phosphotyrosine intensity quantification were generated using MultiExperiment Viewer (version 4.8.1). Average basal pY intensities were plotted for each cell line or genotype. Pathway Map enrichment analysis was performed using GeneGO Pathway Maps in Metacore (Thomson Reuters). Protein interaction analysis was carried out using the Interactome Analysis Workflow tool in Metacore, where significant interactions within sets were identified and used for subsequent Cytoscape network mapping and analysis.

Cytoscape networks and KEGG pathway visualization

Cytoscape (v. 2.8.3) was utilized for visualization of interactions among proteins of the identified phosphorylated peptides, including their degree of connectivity and pY intensity [25]. Network parameter analysis was performed comparing the averaged networks based on genotype using the Network Analysis plugin. Degree of connectivity for each node was visualized by node size. For drug treatment adaptation studies, fold changes in pY intensities were calculated and visualized in network analysis by color-coding. Fold changes less than 0.8 were denoted in green (pY more prominent in basal), and fold changes greater than 1.2 were denoted in pink (pY more prominent in treated cells). Additional pathway analysis for most differentially phosphorylated proteins between control and treatment groups was performed using Kyoto Encyclopedia of Genes and Genomes (KEGG) pathway database.

Statistical Analysis

Results are reported as mean values. GraphPad Prism 6 software was used to calculate the standard error of the mean (SEM) values for pY intensities among individual cell lines in a genotype-based subgroup.

Results

Basal phosphoprotein signaling networks

Seven *BRAF*-mutant melanoma cell lines (1205Lu, WM164, WM793, WM39, WM9, WM239 and WM98A: see Supplemental Figure 1A for mutation information), six *NRAS*-mutant melanoma cell lines (WM1361A, WM1346, WM1366, WM2032, WM3629, WM3670) and one *BRAF/NRAS* wild-type cell line (WM209) were grown to 70% confluency, the tyrosine phosphorylated (pY) peptides captured by immunoprecipitation, and analyzed by mass spectrometry (Figure 1A). Quantification of the tyrosine

phosphorylation using label-free MaxQuant revealed changes in 33-119 distinct peptides, depending upon the cell line (Figures 1B-D: see Supplemental Figure 1A, Supplemental Table 1)[21]. *BRAF*- and *NRAS*-mutant melanoma cell lines were found to exhibit different patterns of peptide phosphorylation (Figure 1B-D). Cytoscape mapping was performed to determine the basal signaling networks across the *BRAF*-mutant melanoma cell line panel (Figure 2A). These analyses revealed a considerable diversity in network complexity, with some cell lines such as WM9 and WM983A showing the greatest number of interactions. Unification of the *BRAF*-mutant data pool revealed the network to consist of 115 nodes, with 472 peptide-peptide interactions (Figure 2B: Supplemental Figure 1B,C). Ranking of these most intense pY peptides, implicated known melanoma signaling pathways including mitogen activated protein kinase (MAPK) (MK01 and MK03), AKT/PI3K (GSK3β), cell cycle regulation (CDK3, CDK1, CDK2, PTTG). Basal phosphorylation of MAPK pathway components and the AKT signaling pathway were confirmed via Western blot (Supplemental Figure 2). Other hubs with high pY intensity common to the majority of *BRAF*-mutant melanoma cell lines are those involved in regulating the cytoskeleton (FAK1, Paxillin, Wiskott-Aldrich syndrome-like (WASL)), protein tyrosine phosphorylation/ dephosphorylation (DYR1A, Dual-Specificity Tyrosine-(Y)-Phosphorylation Regulated Kinase 1A and PTPRA, Protein Tyrosine Phosphatase, Receptor Type, A), interferon signaling (TYK2), RNA splicing (pre-mRNA processing factor 4B, PRP4B) and GTPase function (Ras-Rab interactor-1, RIN1) (Figure 2B-D). We next characterized the basal signaling networks of 6 *NRAS*-mutant melanoma cell lines. Of these, 4 harbored position 61 *NRAS* mutations (WM1361A, WM1346, WM1366, WM2032) and 2 had concurrent position 13 *NRAS* mutations along with low activity *BRAF* mutations (WM3629, WM3670) (Figure 3A and Supplemental Figure 1A). The basal networks of *NRAS*-mutant melanomas were more complex than their *BRAF*-mutant counterparts and showed a similar number of nodes (119 vs. 115) as well as protein-protein interactions (484 vs. 472) (Supplemental Figures 1B,C). Considerable overlap was seen between the peptides with greatest pY intensity for *BRAF*- and *NRAS*-mutant cell lines with cell cycle regulators (CDK1, CDK3, CDK2, PTTG), MAPK components (MK01, MK03), PI3K/AKT signaling (GSK3β) being common to both groups (Figure 3B,C and Supplemental Figure 2). Interestingly, tyrosine phosphorylated regulators of the actin cytoskeleton were less enriched in the *NRAS*- vs. *BRAF*-mutant melanoma (Figure 3C). There were also important differences in the rank order of some pathways, with the PI3K/AKT appearing more important for *NRAS* and the MAPK signaling, particularly ERK2 (MK01) showing greater pY intensity in *BRAF*-mutant melanoma (Figure 2A). Receptor tyrosine kinases (RTKs) and RTK-related proteins, including Axl (UFO), the ERBB2 adaptor LAP2 and the EGF signaling target DCBD2 also emerged as having a greater pY intensity in *NRAS*-mutant melanoma (Figures 3B,C). Despite these differences, GeneGO pathway mapping demonstrated the core pathways of the *BRAF*- and *NRAS*-melanoma cell line panels to show a high degree of similarity (Figures 2D and 3D).

Relatively few *BRAF/NRAS* wild-type cell lines are available. Phosphoproteomic analysis of one such cell line, WM209 demonstrated some similarity in signaling with the *BRAF*- and *NRAS*-mutant melanoma cell lines with constitutive signaling through PI3K/AKT (GSK3β) and MAPK (MK01, ERK2) being observed (Supplemental Figures 3A-C). In common with

both *BRAF*- and *NRAS*-mutant melanoma cell lines, phosphorylation of TYK2, PTTG, DYR1A, and PRP4B were seen. High levels of pY intensity were also observed in multiple RTKs including KIT, IGF1R and c-MET (Supplemental Figures 3A-C).

Adaptive signaling in *BRAF* mutant melanoma cells treated with vemurafenib

To study the adaptive signaling seen following BRAF inhibition we focused upon 1205Lu cells, a line that shows intrinsic resistance to vemurafenib treatment (Figure 4A). Treatment of 1205Lu cells with vemurafenib was associated with increased phosphorylation and signaling through the STAT3 and PI3K/AKT (GSK3α) pathways with increases in focal adhesion signaling (PTK2) also observed (Figure 4A,B). At the same time, vemurafenib treatment decreased phosphorylation of the downstream BRAF targets ERK1 and ERK2, as well as the WNT signaling component β-catenin and phospholipase C1 (PLC1) (Figure 4B). There was also evidence of increased RTK signaling following the addition of drug with increased phosphorylation of Axl/UFO noted (Figure 4B). Validation of the pY data through kinome arrays confirmed the adaptive changes in phosphorylation of AKT, ERK1/2, STAT3, LYN and β-catenin (Figure 4C). Pathway mapping showed BRAF inhibition to be associated with altered signaling through pathways associated with immunity, RTK signaling and cell adhesion (Supplemental Figure 4A). The role of increased PI3K/AKT signaling in the adaptive response to BRAF inhibition was demonstrated through the increased cytotoxic effect seen when BRAF and PI3K was co-targeted (Supplemental Figure 4B). KEGG pathway analysis showed BRAF inhibition to enrich for chemokine signaling in the 1205Lu *BRAF* mutant melanoma cell line (Figure 4D).

Adaptive signaling in *NRAS* mutant melanoma cells following MEK inhibition

MEK inhibitors are the only targeted therapies shown thus far to have any clinical activity against *NRAS*-mutant melanoma. However, responses are typically short-lived and therapeutic escape is common. To explore these adaptations in more detail we focused on the WM1346 cell line. It was noted that although U0126 inhibited phospho-ERK signaling in this cell line, there was little inhibition of growth (Figures 5A,B). This was in contrast to growth inhibition seen in the more sensitive WM1361A *NRAS*-mutant melanoma cell line. Phosphoproteomic analysis showed MEK inhibition to cause a major rewiring of the signaling network resulting in the decreased phosphorylation of ERK1/2 and STAT3 (Figure 5C). At the same time, adaptive increases were noted in EGFR signaling (EGFR, LAP2 and Shc1), Src family kinases (Fyn) and protein kinase Cδ (PRKCD) (Figure 5C). Decreases in phosphorylation were also noted in many proteins implicated in cytoskeletal/focal adhesion regulation including vimentin, paxillin, delta catenin, drebrin-like protein (Figure 5A). GeneGO analysis confirmed the changes in these pathways and revealed MEK inhibition to alter signaling to the cytoskeleton, the EGFR pathway, integrin mediated adhesion, the JAK/STAT pathway and chemotaxis (Supplemental Figure 5A). KEGG pathway analysis showed MEK inhibition to enrich for focal adhesion signaling in the WM1346 *NRAS*-mutant melanoma cell line (Figure 5D). In line with the expected effects of MEK inhibition upon the cytoskeleton, treatment of WM1346 cells with U0126 increased actin stress fiber formation and reduced migration in a scratch wound assay (Supplemental Figures 5B,C).

Discussion

Emerging evidence suggests that oncogene-driven signaling networks are highly dynamic and subject to rewiring following drug treatment. Although poorly characterized at a systems level, these adaptations play a key role in therapeutic escape. Precedents for the rational identification of combination therapy partners already exist with previous work from our lab and others demonstrating BRAF inhibition to be associated with the recovery of signaling in the MAPK pathway, which can be overcome through the vertical pathway targeting of BRAF and MEK [14]. Similarly, in some *BRAF*-mutant melanoma cell lines, BRAF and MEK inhibitor treatment is associated with adaptive PI3K/AKT signaling that also limits the cytotoxic response [23, 26]. Our group has also recently begun to characterize drug-mediated signaling adaptation using quantitative liquid chromatography multiple reaction monitoring (LC-MRM) [27].

Melanomas are known to be very genetically heterogeneous tumors with the phosphoproteomic analysis demonstrating a great diversity of tyrosine phosphorylated peptides between the cell lines [6]. Despite this expectation, a set of peptides was identified with constitutive phosphorylation across the majority of the cell types analyzed. A pathway level analysis also suggested that both *BRAF*- and *NRAS*-mutant melanoma cell lines were dependent upon a similar series of pathways. Many of the core peptides were involved in processes required for tumor maintenance such as cell cycle regulation, cytoskeletal rearrangement/invasion, and tyrosine phosphorylation/dephosphorylation. Commonalities were also noted in the phosphorylation of peptides involved in the signaling pathways driving melanoma progression; the MAPK pathway and the PI3K/AKT signaling pathway [28-30]. The MAPK signaling pathway plays a pivotal role in the oncogenic behavior of melanoma in part through its effects upon growth (via the regulation of cyclin D1 expression), increased cell survival (negative regulation of pro-apoptotic proteins) and metastasis (through the regulation of the actin cytoskeleton and matrix metalloproteinase (MMP) expression) [31-34]. Despite MAPK pathway drivers such as mutant BRAF being an early event in melanomagenesis, constitutive ERK activation cannot initiate and sustain melanoma growth alone, with parallel signals also required through the PI3K/AKT pathway [35, 36]. Evidence for activity in the PI3K/AKT pathway was suggested by the constitutive phosphorylation of GSK3β at Y216. GSK3β is a regulator of glycogen metabolism and a downstream target of AKT (which phosphorylates the protein at S9 leading to its inactivation). Previous studies from our lab have shown GSK3β to be phosphorylated in the majority of all melanoma cell lines, and to be a good surrogate marker of AKT activity [37].

Despite the variability in pY peptides being quite high at the cell line level, genetic sub-type specific differences in the pY profile were noted. *NRAS*-mutant melanoma cell lines exhibited a greater intensity in the level of RTK phosphorylation than cell lines harboring *BRAF* mutations, particularly sites on EGFR and Axl. These findings agree with previous studies that showed the constitutive phosphorylation of Axl at Y696 in most of the *NRAS*-mutant melanoma cell lines that was lacking in cell lines harboring *BRAF* mutations [38, 39]. In melanoma cells, Axl signals through the AKT pathway leading to increased melanoma cell migration and invasion [38]. Other RTKs with constitutive tyrosine phosphorylation in the *NRAS*-mutant melanoma cell lines included EGFR, a wide spectrum

of ephrins (EphA2, EphA4 and EphB2) and c-MET. There is already some evidence that *NRAS*-mutant melanomas have an increased dependency upon c-MET signaling, and that expression of c-MET is directly regulated through mutant *NRAS* [40]. Support for the role of EGFR in *NRAS*-mutant melanoma came from the high constitutive levels of tyrosine phosphorylation of EGFR-related signaling targets such as DCBD2, and the ERBB2 adaptor protein, LAP2. Recent studies have also shed light upon why RTK signaling may be less important for the tumorigenic behavior of *BRAF*-mutant melanoma than those that are *BRAF* wild-type. Under basal conditions, a high level of feedback inhibition within the MAPK pathway suppressed signals emanating from RTK-mediated Ras signaling [13]. In situations where BRAF signaling was inhibited, such as following vemurafenib treatment, the feedback inhibition in the pathway was relieved, allowing the cells to respond to growth factor signals [13].

NRAS-mutant melanoma cell lines showed less phosphorylation of peptides involved in regulation of the cytoskeleton than their *BRAF*-mutant counterparts. The role of oncogenic *BRAF* in regulating the invasive behavior of melanoma cells has been well characterized with studies implicating the RND3-mediated regulation of the Rho/Rock/LIM kinase/Cofilin pathways [33]. Additional work has shown a role for mutant BRAF in the release of cytosolic calcium secondary to the inhibition of cyclic GMP phosphodiesterase PDE5A, with increases in cell contractility being mediated through MLC2 [34]. Although not explored as extensively, Ras may regulate cell motility in different ways - such as through direct modulation of small G-proteins involved in cytoskeletal control like Rho, Rac and CDC42 [41].

There is a growing realization that oncogene-driven signaling networks are highly plastic and adapt rapidly to addition of kinase inhibitors or the silencing of the driver mutation. This phenomenon has been studied most extensively in epithelial cancers. In colorectal carcinoma, the escape from the shRNA knockdown of *KRAS* leads to increased AKT signaling and can be mediated through IGF1R [42]. In this instance, loss of KRAS signaling decreases signaling through the MAPK pathway leading to decreased feedback inhibition mediated through IRS-1 [42]. In triple negative breast cancer, the inhibition of MEK is associated with reactivation of signaling that occurs through the increased expression of multiple RTKs [43]. Treatment of *BRAF*- and *NRAS*-mutant melanoma cell lines with BRAF and MEK inhibitors, respectively, led to a rewiring of the signaling networks. In the *BRAF*-mutant 1205Lu melanoma cell line, adaptive signaling through the PI3K and STAT3 signaling pathways were observed, both of which have been implicated in therapeutic escape. We here provide evidence that treatment of 1205Lu cells with a combination of a BRAF and a PI3K inhibitor is associated with increased cytotoxicity compared to either inhibitor alone. Adaptive STAT3 signaling has been previously reported in melanoma cells treated with MEK inhibitors, where it drives invasion [44]. Some studies have also suggested that increased STAT3 signaling can mediate acquired resistance to vemurafenib and may even help melanoma cells to evade the immune system [45, 46]. Treatment of melanoma cells with BRAF or MEK inhibitors is known to affect focal adhesion dynamics leading to the formation of actin stress fibers. There is also evidence that MEK inhibition directly inhibits the phosphorylation of the cytoskeletal regulator MINEVRA/FAM129 in

BRAF-mutant melanoma leading to inhibition of cell motility [17]. Analysis of the phosphotyrosine data showed BRAF inhibition to be associated with increased phosphorylation of PTK2, a possible mediator of these cytoskeletal effects.

In a similar vein to other published studies, inhibition of MEK in the WM1346 *NRAS*-mutant melanoma cell line led to adaptive RTK signaling mediated through EGFR. In colorectal carcinoma, a feedback loop mediated through EGFR drives resistance to BRAF inhibitors that can be overcome through dual targeting with Erlotinib and vemurafenib [47]. Both Src and EGFR signaling have also been associated with acquired BRAF inhibitor resistance in melanoma [48]. Other signal transduction molecules with a potential role in therapeutic escape include PKCδ, which has been implicated in tamoxifen resistance in breast cancer as well as doxorubicin resistance [49, 50]. Like the adaptive signaling in BRAF inhibitor treated cells, MEK inhibition in *NRAS*-mutant melanoma cells also led to changes in the phosphorylation of cytoskeletal proteins, and was associated with increased actin stress fiber formation and reduced motility [17]. Together, these data suggest that even if *NRAS*-mutant melanomas are not growth inhibited following MEK inhibition, there may be some benefit in terms of reduced tumor invasion.

The development of personalized targeted therapy combinations will require strategies that can interrogate the adaptive signaling responses in patients on therapy. Platforms such as mass spectrometry-based phosphoproteomics will prove key in characterizing both the basal signaling networks and identifying the hubs that need to be targeted to prevent therapeutic escape. The continued development of these technologies and their further application to clinical specimens will allow treatment strategies to be refined and further personalized leading to more durable responses for melanoma patients.

Supplementary Material

Refer to Web version on PubMed Central for supplementary material.

Acknowledgments

Work in the Smalley lab is supported by R01 CA161107 and SPORE grant P50 CA168536-01A1 from the National Institutes of Health. Inna Fedorenko was supported by a grant from the Joanna M. Nicolay Melanoma Foundation. The Moffitt Proteomics Facility is supported by the US Army Medical Research and Materiel Command (W81XWH-08-2-0101) for a National Functional Genomics Center, the National Cancer Institute (P30-CA076292) as a Cancer Center Support Grant, and the Moffitt Foundation.

References

[1]. Flaherty KT, Infante JR, Daud A, Gonzalez R, et al. Combined BRAF and MEK inhibition in melanoma with BRAF V600 mutations. The New England journal of medicine. 2012; 367:1694–1703. [PubMed: 23020132]

[2]. Flaherty KT, Robert C, Hersey P, Nathan P, et al. Improved survival with MEK inhibition in BRAF-mutated melanoma. The New England journal of medicine. 2012; 367:107–114. [PubMed: 22663011]

[3]. Van Allen EM, Wagle N, Sucker A, Treacy DJ, et al. The genetic landscape of clinical resistance to RAF inhibition in metastatic melanoma. Cancer Discov. 2014; 4:94–109. [PubMed: 24265153]

[4]. Smalley KS, Nathanson KL, Flaherty KT. Genetic subgrouping of melanoma reveals new opportunities for targeted therapy. Cancer Res. 2009; 69:3241–3244. [PubMed: 19351826]

[5]. Davies H, Bignell GR, Cox C, Stephens P, et al. Mutations of the BRAF gene in human cancer. Nature. 2002; 417:949–954. [PubMed: 12068308]

[6]. Hodis E, Watson IR, Kryukov GV, Arold ST, et al. A Landscape of Driver Mutations in Melanoma. Cell. 2012; 150:251–263. [PubMed: 22817889]

[7]. Fedorenko IV, Gibney GT, Smalley KS. NRAS mutant melanoma: biological behavior and future strategies for therapeutic management. Oncogene. 2013; 32:3009–3018. [PubMed: 23069660]

[8]. Ascierto PA, Schadendorf D, Berking C, Agarwala SS, et al. MEK162 for patients with advanced melanoma harbouring NRAS or Val600 BRAF mutations: a non-randomised, open-label phase 2 study. The lancet oncology. 2013; 14:249–256. [PubMed: 23414587]

[9]. Rebecca VW, Massaro RR, Fedorenko IV, Sondak VK, et al. Inhibition of autophagy enhances the effects of the AKT inhibitor MK-2206 when combined with paclitaxel and carboplatin in BRAF wild-type melanoma. Pigm Cell Melanoma R. 2014; 27:465–478.

[10]. Berger MF, Hodis E, Heffernan TP, Deribe YL, et al. Melanoma genome sequencing reveals frequent PREX2 mutations. Nature. 2012; 485:502–506. [PubMed: 22622578]

[11]. Wagle N, Van Allen EM, Treacy DJ, Frederick DT, et al. MAP kinase pathway alterations in BRAF-mutant melanoma patients with acquired resistance to combined RAF/MEK inhibition. Cancer Discov. 2014; 4:61–68. [PubMed: 24265154]

[12]. Chandarlapaty S, Sawai A, Scaltriti M, Rodrik-Outmezguine V, et al. AKT inhibition relieves feedback suppression of receptor tyrosine kinase expression and activity. Cancer Cell. 2011; 19:58–71. [PubMed: 21215704]

[13]. Lito P, Pratilas CA, Joseph EW, Tadi M, et al. Relief of Profound Feedback Inhibition of Mitogenic Signaling by RAF Inhibitors Attenuates Their Activity in BRAFV600E Melanomas. Cancer Cell. 2012; 22:668–682. [PubMed: 23153539]

[14]. Paraiso KH, Fedorenko IV, Cantini LP, Munko AC, et al. Recovery of phospho-ERK activity allows melanoma cells to escape from BRAF inhibitor therapy. Br J Cancer. 2010; 102:1724–1730. [PubMed: 20531415]

[15]. Paraiso KH, Haarberg HE, Wood E, Rebecca VW, et al. The HSP90 inhibitor XL888 overcomes BRAF inhibitor resistance mediated through diverse mechanisms. Clinical cancer research : an official journal of the American Association for Cancer Research. 2012; 18:2502–2514. [PubMed: 22351686]

[16]. Acquaviva J, Smith DL, Jimenez JP, Zhang C, et al. Overcoming acquired BRAF inhibitor resistance in melanoma via targeted inhibition of Hsp90 with ganetespib. Molecular Cancer Therapeutics. 2014; 13:353–363. [PubMed: 24398428]

[17]. Old WM, Shabb JB, Houel S, Wang H, et al. Functional proteomics identifies targets of phosphorylation by B-Raf signaling in melanoma. Molecular cell. 2009; 34:115–131. [PubMed: 19362540]

[18]. Kirkpatrick DS, Bustos DJ, Dogan T, Chan J, et al. Phosphoproteomic characterization of DNA damage response in melanoma cells following MEK/PI3K dual inhibition. Proceedings of the National Academy of Sciences of the United States of America. 2013; 110:19426–19431. [PubMed: 24218548]

[19]. Rush J, Moritz A, Lee KA, Guo A, et al. Immunoaffinity profiling of tyrosine phosphorylation in cancer cells. Nature Biotechnology. 2005; 23:94–101.

[20]. Li J, Rix U, Fang B, Bai Y, et al. A chemical and phosphoproteomic characterization of dasatinib action in lung cancer. Nat Chem Biol. 2010; 6:291–299. [PubMed: 20190765]

[21]. Cox J, Mann M. MaxQuant enables high peptide identification rates, individualized p.p.b.-range mass accuracies and proteome-wide protein quantification. Nature Biotechnology. 2008; 26:1367–1372.

[22]. Cox J, Matic I, Hilger M, Nagaraj N, et al. A practical guide to the MaxQuant computational platform for SILAC-based quantitative proteomics. Nat Protoc. 2009; 4:698–705. [PubMed: 19373234]

[23]. Paraiso KH, Xiang Y, Rebecca VW, Abel EV, et al. PTEN loss confers BRAF inhibitor resistance to melanoma cells through the suppression of BIM expression. Cancer Research. 2011; 71:2750–2760. [PubMed: 21317224]

[24]. Paraiso KH, Xiang Y, Rebecca VW, Abel EV, et al. PTEN loss confers BRAF inhibitor resistance to melanoma cells through the suppression of BIM expression. Cancer Res. 2011; 71:2750–2760. [PubMed: 21317224]

[25]. Smoot ME, Ono K, Ruscheinski J, Wang PL, Ideker T. Cytoscape 2.8: new features for data integration and network visualization. Bioinformatics. 2011; 27:431–432. [PubMed: 21149340]

[26]. Gopal YN, Deng W, Woodman SE, Komurov K, et al. Basal and treatment-induced activation of AKT mediates resistance to cell death by AZD6244 (ARRY-142886) in Braf-mutant human cutaneous melanoma cells. Cancer Res. 2010; 70:8736–8747. [PubMed: 20959481]

[27]. Rebecca VW, Wood ER, Fedorenko IV, Paraiso KH, et al. Evaluating Melanoma Drug Response and Therapeutic Escape with Quantitative Proteomics. Molecular & cellular proteomics : MCP. 2014

[28]. Smalley KSM. A pivotal role for ERK in the oncogenic behaviour of malignant melanoma? International Journal of Cancer. 2003; 104:527–532.

[29]. Fedorenko IV, Paraiso KH, Smalley KS. Acquired and intrinsic BRAF inhibitor resistance in BRAF V600E mutant melanoma. Biochem Pharmacol. 2011; 82:201–209. [PubMed: 21635872]

[30]. Madhunapantula SV, Robertson GP. The PTEN-AKT3 signaling cascade as a therapeutic target in melanoma. Pigment Cell Melanoma Res. 2009; 22:400–419. [PubMed: 19493313]

[31]. Bhatt KV, Spofford LS, Aram G, McMullen M, et al. Adhesion control of cyclin D1 and p27Kip1 levels is deregulated in melanoma cells through BRAF-MEK-ERK signaling. Oncogene. 2005; 24:3459–3471. [PubMed: 15735667]

[32]. Boisvert-Adamo K, Aplin AE. Mutant B-RAF mediates resistance to anoikis via Bad and Bim. Oncogene. 2008; 27:3301–3312. [PubMed: 18246127]

[33]. Klein RM, Aplin AE. Rnd3 regulation of the actin cytoskeleton promotes melanoma migration and invasive outgrowth in three dimensions. Cancer Res. 2009; 69:2224–2233. [PubMed: 19244113]

[34]. Arozarena I, Sanchez-Laorden B, Packer L, Hidalgo-Carcedo C, et al. Oncogenic BRAF induces melanoma cell invasion by downregulating the cGMP-specific phosphodiesterase PDE5A. Cancer Cell. 2011; 19:45–57. [PubMed: 21215707]

[35]. Vredeveld LC, Possik PA, Smit MA, Meissl K, et al. Abrogation of BRAFV600E-induced senescence by PI3K pathway activation contributes to melanomagenesis. Gene Dev. 2012; 26:1055–1069. [PubMed: 22549727]

[36]. Dankort D, Curley DP, Cartlidge RA, Nelson B, et al. Braf(V600E) cooperates with Pten loss to induce metastatic melanoma. Nat Genet. 2009; 41:544–552. [PubMed: 19282848]

[37]. John JK, Paraiso KH, Rebecca VW, Cantini LP, et al. GSK3beta Inhibition Blocks Melanoma Cell/Host Interactions by Downregulating N-Cadherin Expression and Decreasing FAK Phosphorylation. The Journal of investigative dermatology. 2012; 132:2818–2827. [PubMed: 22810307]

[38]. Sensi M, Catani M, Castellano G, Nicolini G, et al. Human Cutaneous Melanomas Lacking MITF and Melanocyte Differentiation Antigens Express a Functional Axl Receptor Kinase. The Journal of investigative dermatology. 2011; 131:2448–2457. [PubMed: 21796150]

[39]. Tworkoski K, Singhal G, Szpakowski S, Zito CI, et al. Phosphoproteomic screen identifies potential therapeutic targets in melanoma. Molecular cancer research : MCR. 2011; 9:801–812. [PubMed: 21521745]

[40]. Chattopadhyay C, Ellerhorst JA, Ekmekcioglu S, Greene VR, et al. Association of activated c-Met with NRAS-mutated human melanomas: a possible avenue for targeting. International Journal of Cancer. 2012; 131:E56–E65.

[41]. Malumbres M, Barbacid M. RAS oncogenes: the first 30 years. Nature reviews. Cancer. 2003; 3:459–465.

[42]. Ebi H, Corcoran RB, Singh A, Chen Z, et al. Receptor tyrosine kinases exert dominant control over PI3K signaling in human KRAS mutant colorectal cancers. Journal of Clinical Investigation. 2011; 121:4311–4321. [PubMed: 21985784]

[43]. Duncan JS, Whittle MC, Nakamura K, Abell AN, et al. Dynamic reprogramming of the kinome in response to targeted MEK inhibition in triple-negative breast cancer. Cell. 2012; 149:307–321. [PubMed: 22500798]

[44]. Vultur A, Villanueva J, Krepler C, Rajan G, et al. MEK inhibition affects STAT3 signaling and invasion in human melanoma cell lines. Oncogene. 2014; 33:1850–1861. [PubMed: 23624919]

[45]. Jiang X, Zhou J, Giobbie-Hurder A, Wargo J, Hodi FS. The activation of MAPK in melanoma cells resistant to BRAF inhibition promotes PD-L1 expression that is reversible by MEK and PI3K inhibition. Clinical cancer research : an official journal of the American Association for Cancer Research. 2013; 19:598–609. [PubMed: 23095323]

[46]. Liu F, Cao J, Wu J, Sullivan K, et al. Stat3-targeted therapies overcome the acquired resistance to vemurafenib in melanomas. The Journal of investigative dermatology. 2013; 133:2041–2049. [PubMed: 23344460]

[47]. Prahallad A, Sun C, Huang S, Di Nicolantonio F, et al. Unresponsiveness of colon cancer to BRAF(V600E) inhibition through feedback activation of EGFR. Nature. 2012; 483:100–103. [PubMed: 22281684]

[48]. Girotti MR, Pedersen M, Sanchez-Laorden B, Viros A, et al. Inhibiting EGF Receptor or SRC Family Kinase Signaling Overcomes BRAF Inhibitor Resistance in Melanoma. Cancer Discov. 2013; 3:158–167. [PubMed: 23242808]

[49]. Nabha SM, Glaros S, Hong M, Lykkesfeldt AE, et al. Upregulation of PKC-delta contributes to antiestrogen resistance in mammary tumor cells. Oncogene. 2005; 24:3166–3176. [PubMed: 15735693]

[50]. Diaz Bessone MI, Berardi DE, Campodonico PB, Todaro LB, et al. Involvement of PKC delta (PKCdelta) in the resistance against different doxorubicin analogs. Breast Cancer Research and Treatment. 2011; 126:577–587. [PubMed: 20512658]

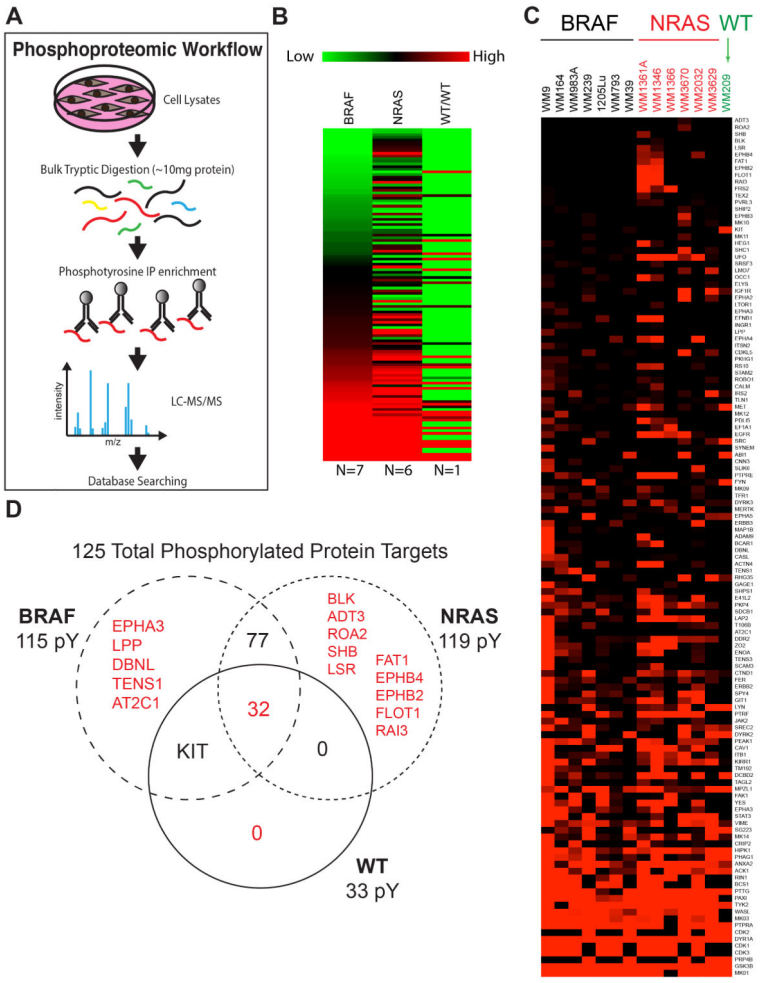

Figure 1. Phosphoproteomic analysis of melanoma cell lines based on genotype

A: Workflow of the phosphoproteomic experiment. **B:** Heat map showing average pY intensities summarized for three melanoma cell line genotypes. Seven *BRAF*-mutant melanoma cell lines include WM9, WM164, WM983A, WM239, 1205Lu, WM793, and WM39. Six *NRAS*-mutant melanoma cell lines include WM1361A, WM1346, WM1366, WM3670, WM2032, and WM3629. One cell line, WM209, with wild type *NRAS* and *BRAF* was analyzed. **C:** Heat map showing average pY intensities for each cell line. **D:** Venn diagram depicts the breakdown of the number of phosphorylated proteins that are unique to each genotype and common among genotypes.

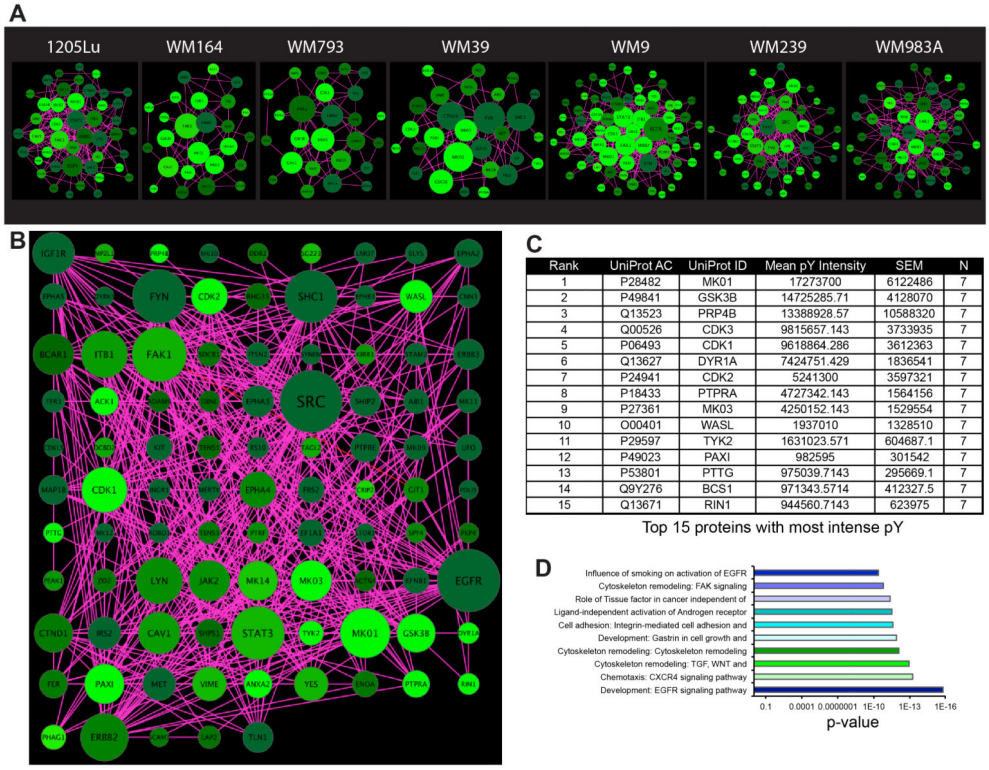

Rank	UniProt AC	UniProt ID	Mean pY Intensity	SEM	N
1	P28482	MK01	17273700	6122486	7
2	P49841	GSK3B	14725285.71	4128070	7
3	Q13523	PRP4B	13388928.57	10588320	7
4	Q00526	CDK3	9815657.143	3733935	7
5	P06493	CDK1	9618864.286	3612363	7
6	Q13627	DYR1A	7424751.429	1836541	7
7	P24941	CDK2	5241300	3597321	7
8	P18433	PTPRA	4727342.143	1564156	7
9	P27361	MK03	4250152.143	1529554	7
10	O00401	WASL	1937010	1328510	7
11	P29597	TYK2	1631023.571	604687.1	7
12	P49023	PAXI	982595	301542	7
13	P53801	PTTG	975039.7143	295669.1	7
14	Q9Y276	BCS1	971343.5714	412327.5	7
15	Q13671	RIN1	944560.7143	623975	7

Figure 2. *BRAF*-mutant melanoma signaling

A: Cytoscape networks depicting the basal interactome for each cell line. Networks were visualized based on degree of connectivity (node size), and average pY intensity (node color, brighter = higher intensity values). **B:** A unified Cytoscape network depicting the average interactome for the *BRAF*-mutant genotype. Networks were visualized based on degree of connectivity (node size), and average pY intensity (node color, brighter = higher intensity values). Phosphopeptide intensities were calculated based on mean values among all cell lines in the subgroup. Due to overly high connectivity of SRC, its node size was limited by a threshold reflecting the largest size of the next most connected hub in order to highlight the differences in connectivity of the rest of the hubs in the network. **C:** Table of the 15 proteins containing phosphorylated peptides with the highest intensities in the *BRAF*-mutant cell line group, based on mean pY intensities. **D:** Top ten highly enriched Metacore pathway maps for the *BRAF*-mutant cell line group.

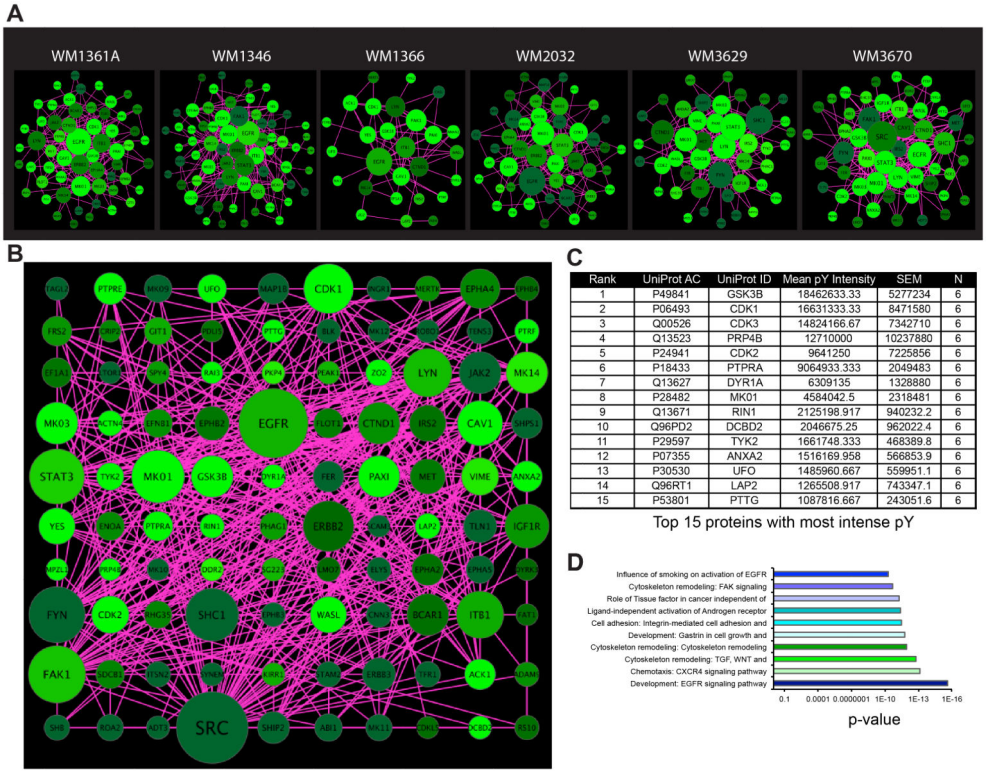

Figure 3. *NRAS*-mutant melanoma signaling

A: Cytoscape networks depicting the basal interactome for each cell line. Networks were visualized based on degree of connectivity (node size), and average pY intensity (node color, brighter = higher intensity values). **B:** A unified Cytoscape network depicting the average interactome for the *NRAS*-mutant genotype. Networks were visualized based on degree of connectivity (node size), and average pY intensity (node color, brighter = higher intensity values). Phosphopeptide intensities were calculated based on mean values among all cell lines in the subgroup. Due to overly high connectivity of SRC, its node size was limited by a threshold reflecting the largest size of the next most connected hub in order to highlight the differences in connectivity of the rest of the hubs in the network. **C:** Table of the 15 proteins containing the most intense phosphorylated peptides in the *NRAS*-mutant cell line group, based on mean pY intensities. **D:** Top ten highly enriched Metacore pathway maps for the *NRAS*-mutant cell line group.

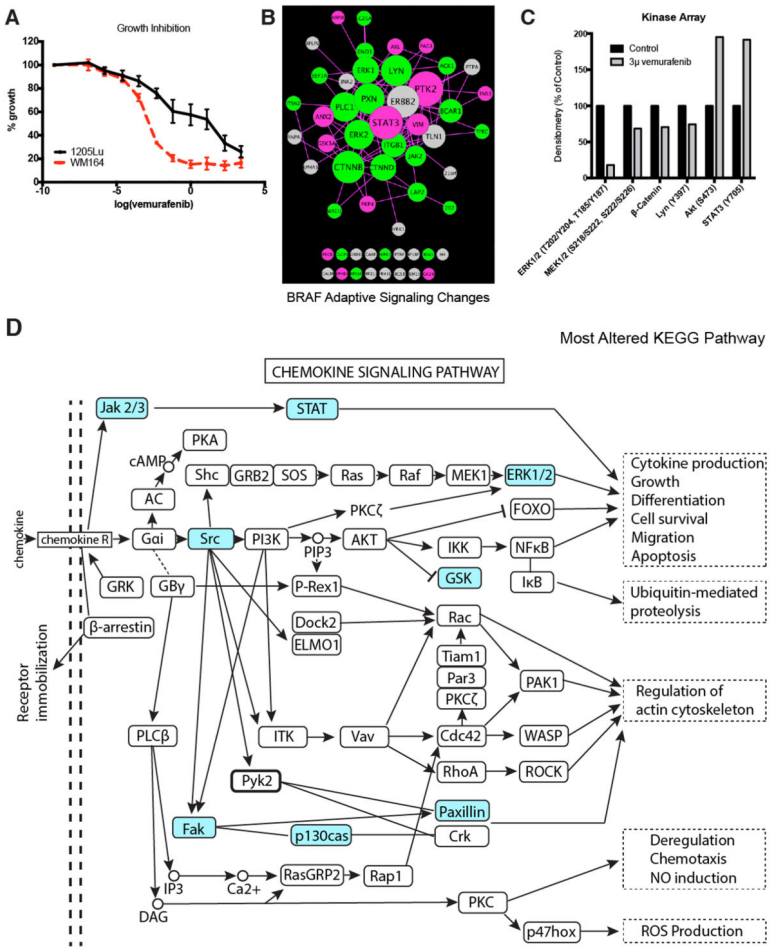

Figure 4. Adaptive signaling in *BRAF*-mutant melanoma cell line

A: Treatment of WM164 (sensitive) and 1205Lu (partly resistant) *BRAF*-mutant melanoma cell lines with vemurafenib leads to the inhibition of growth. Cells were treated with drug for 72 hours before being analyzed using the MTT assay. **B:** The 1205Lu *BRAF*^{V600E} melanoma cell line was treated with 3μM vemurafenib for 24 hours, then analyzed by phosphoproteomics and compared against the basal signaling in the same cells. The signaling network was visualized using Cytoscape based on degree of connectivity (node size), and average fold change in pY intensity (node color, brighter = higher intensity values). Fold changes less than 0.8 are denoted in green (pY more prominent in basal), and fold changes greater than 1.2 are denoted in pink (pY more prominent in treated cells). **C:** Validation of the MS data from (B) using a kinome array. 1205Lu cells were treated with 3μM vemurafenib for 24 hrs. before phosphorylation levels of ERK, MEK, β-catenin, Ly, AKT and STAT3 were quantified using the kinome array. **D:** Kyoto Encyclopedia of Genes and Genomes (KEGG) pathway analysis on proteins characterized as greatly altered identified chemokine signaling pathway to be most affected by vemurafenib treatment. Proteins identified to have a change in pY that are 0.8-fold and less, or those that are 1.2-fold or higher were categorized as altered (highlighted in blue).

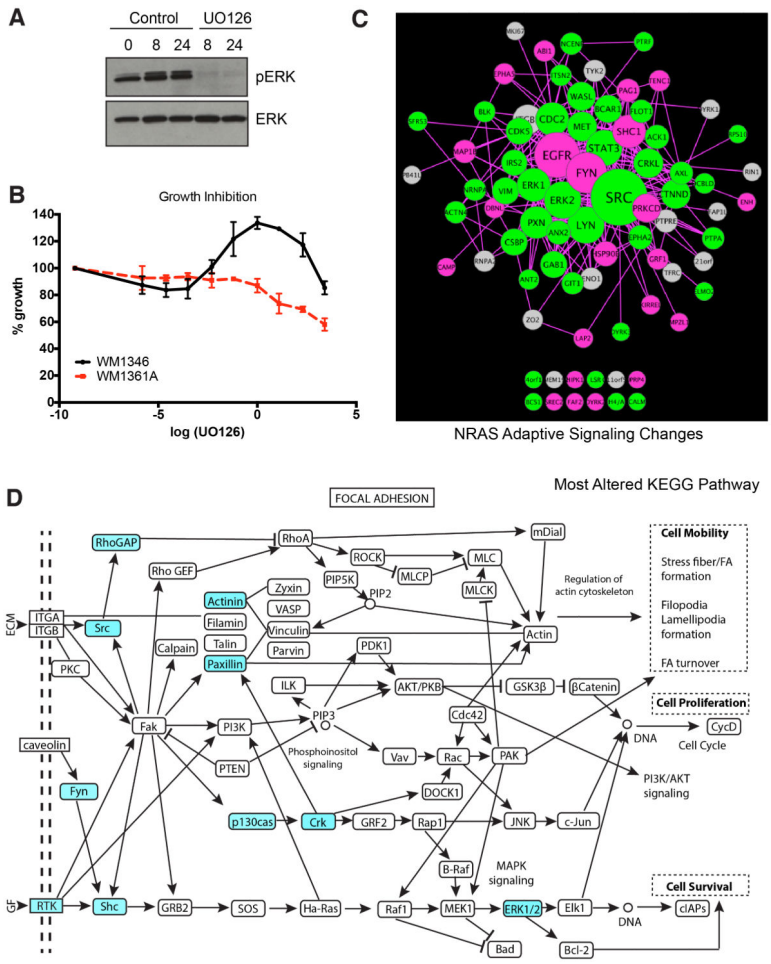

Figure 5. Adaptive signaling in *NRAS*-mutant melanoma cell line

A: U0126 inhibits phospho-ERK signaling. WM1346 cells were treated with U0126 (10 μM) for 0-24 hours. Western blot shows phospho-ERK and total ERK. **B:** U0126 has limited growth inhibitory effects on WM1346 cells. WM1346 and WM1361A cells were treated with increasing concentrations of U0126 for 72 hrs. before being analyzed using the MTT assay. **C:** WM1346 cells were treated with 10μM UO126 for 24 hours, then analyzed by phosphoproteomics for comparison to basal signaling. The signaling network was visualized using Cytoscape based on degree of connectivity (node size), and average fold change in pY intensity (node color, brighter = higher intensity values). Fold changes less than 0.8 are denoted in green (pY more prominent in basal), and fold changes greater than 1.2 are denoted in pink (pY more prominent in treated cells). **D:** Kyoto Encyclopedia of Genes and Genomes (KEGG) pathway analysis on proteins characterized as greatly altered identified focal adhesion signaling pathway most affected by the Mek inhibitor treatment. Proteins identified to have a change in pY that are 0.8-fold and less, or those that are 1.2-fold or higher were categorized as altered (highlighted in blue).